N84-29147

# MONTHLY PROGRSS REPORT NO. 12
# FOR MAY 1984

# SRB/FWC WATER IMPACT - FLEXIBLE BODY LOADS TEST

June 1984

Prepared for:

Dennis Kross, ED22
National Aeronautics and Space Administration
George C. Marshall Space Flight Center
Marshall Space Flight Center, AL 35812

Prepared by:

Bolt Beranek and Newman Inc.
10 Moulton Street
Cambridge, MA 02238

During the May reporting period, BBN efforts were concentrated on two technical areas:

1. Evaluation of potential correction methods for spurious case strain outputs from the pressure transducers during the NSWC tests.

2. Assessing procedures for modifying either the excitation function or the response function to account for hydro-elastic effects.

## 1. Case Strain Corrections

The quick-look analysis of the data measured during the quarter scale FWC drop tests at NSWC indicated a potential problem with the cavity collapse pressure measurements. The problem surfaced when NASA noticed that in many tests there was a non-physical negative pressure precursor just prior to the arrival of the cavity collapse pressure pulse. Possible causes for the spurious pressure included acceleration and case strain sensitivity of the pressure transducers. Since a series of acceleration sensitivity tests conducted by NASA proved the acceleration sensitivity to be unimportant, attention was focused on case strain. The case strain outputs appear to be caused by insufficient clearance between the machined hard nylon fiberglass impregnated mounting fixtures and the transducer case near the diaphragm. This lack of clearance caused a pinching of the diaphragm particularly in tests of the flexible configurations (e.g., III, IV, V) where there was significant deformation of the case. In an effort to estimate an upper bound for the case strain output, we presented the problem to the manufacturer (PCB) and NASA ran a series of case strain sensitivity tests. Lou Zagszt confirmed our suspicion that PCB had not quantified case strain output. Unfortunately, there are no standard tests for case strain sensitivity since the output is critically dependent

on the local strain field. The NASA tests attempted to determine a single factor for adjusting the results from all transducers. Unfortunately, these test results again demonstrated the difficulty in correcting for case strain, i.e., there was an order of magnitude difference in the correction factors for individual transducers. The definition of a single correction factor applicable to all transducers seems unlikely.

On the other hand, the tests of the stiffer configurations I and II may provide a reasonable estimation of the excitation function. We will return to the case strain issue after we have developed some additional tools for handling the hydroelastic effects.

## 2. Hydroelastic Effects

The response of the FWC shell to the hydrodynamic loads caused by cavity collapse is represented by a differential equation of the form

$$L(\omega) = \rho h \ddot{\omega} + P_T \qquad (1)$$

where $\omega$ is the radial deflection, L is a differential operator, and $P_T$ is the pressure applied by the collapsing cavity. The pressure P can be broken into two parts; see Ref. 1 for example.

$$P_T = P_\infty + \sum_n P_H \qquad (2)$$

where the $P_\infty$ term represents the pressure that would be applied to a rigid body and the $\sum_n P_H$ are the pressures that result from the motions of the body in the fluid in each of the modes n. The latter term is, of course, the "hydroelastic effect." The sum of the two terms $P_T$ is the pressure measured on the surface of the shell during any of the drop tests. It is this measured pressure, barring spurious case strain outputs, that should be applied as the excitation in the finite element model representation of the quarter scale tests.

This measured pressure, however, cannot be directly scaled to the full scale flight vehicle loads since neither the water nor the quarter scale segment was elastically scaled, and, consequently, the pressure $\sum_n P_H$ in Eq. 2 will not be properly scaled.

In order to provide a proper full scale load, we must:

- remove the hydroelastic effects from the measured quarter scale pressures,
- scale the rigid body pressures, $P_\infty$ in Eq. 2., and
- impose corrections that account for the hydroelastic response of the full scale flight vehicle.

Once we have successfully used the measured quarter scale pressures in the finite element model to predict the measured response, we should evaluate the procedure for incorporating hydroelastic effects by:

- developing a new pressure loading from scaled 8% or flight data,
- including an appropriate hydroelastic correction, and
- applying this pressure to again predict the response of the quarter scale model.

We emphasize that it is mandatory to apply all corrections to the excitation function rather than to the structure since application to the structural matrices would require a recalculation of the normal modes and frequencies after each interval in time and become extremely costly and time consuming.

Let us consider the hydrodynamic correction in more detail. Reference 2 indicates that in the case of plane motion of a cylindrical or axisymmetric motion of a spherical shell, the modal pressures can be expressed by a convolution of the acceleration of the shell relative to the water and a resistance function $\psi_n(t)$.

$$P_n(t) = \rho c \int_o^t [\ddot{\omega}_n(\tau) - \dot{U}_n(\tau)]\ \psi_n(t-\tau)\ d\tau \qquad (3)$$

where $\rho c$ is the acoustic impedance of the water

$\ddot{\omega}$ is the local acceleration of the shell and

$\dot{U}_n$ is the local acceleration of a water particle at the shell surface;

also

$$\lim_{t\to o} \psi_n(t) = \lim_{t\to\infty} \psi_n(t) = 0$$

$$\lim_{t\to\infty} \int_o^t \psi_n(\tau)d\tau = (m_v)_n/\rho c$$

where $(m_v)_n$ will be called the virtual mass.

A useful approximation for $\psi_n$ that satisfies these conditions is

$$\psi_n(t) = e^{-[\rho c/(m_v)_n]t}$$

Substituting this value for $\psi$ into the convolution integral (3) gives

$$P_n(t) = \rho c \int_o^t [\ddot{\omega}_n(\tau) - \dot{U}_n(\tau)]e^{\frac{-\rho c}{(m_v)_n}(t-\tau)}\ d\tau \qquad (4)$$

The Laplace transform of Eq. 4 is

$$P_n(s)=\rho c[s^2\omega_n(s)-s\omega_n(o)-\dot{\omega}_n(o)-s^1u(s)+u_n(o)]\frac{1}{[s+\frac{\rho c}{(m_v)_n}]} \qquad (5)$$

The initial conditions provide some simplifications to Eq. 4 since the inital displacement is zero.

$$\omega_n(o) = 0$$

and also, since the initial velocity is the same for both

$$\dot{\omega}_n(o) - u_n(o) = 0$$

Equation 5 reduces to

$$P_n(s) = \rho c[s^2\omega_n(s) - su_n(s)]\frac{1}{\left(s+\frac{\rho c}{(m_v)_n}\right)} \tag{6}$$

Consider now both short and long term solutions to Eq. 6. For short times, s is large and $s>>\frac{\rho c}{(m_v)_n}$; therefore,

$$P_n(s) = \rho c[s\omega_n(s) - u_n(s)] \tag{7}$$

The inverse Laplace transform of Eq. 7 is

$$P_n(t) = \rho c[\dot{\omega}_n - u_n] \tag{8}$$

For long times, s is small and $s<<\frac{\rho c}{(m_v)_n}$ and Eq. 6 reduces to

$$P_n(s) = (m_v)_n[s^2\omega(s) - su(s)] \tag{9}$$

The inverse Laplace transform of Eq. 9 is

$$P_n(t) = (m_v)_n[\ddot{\omega} - \dot{u}_n] \tag{10}$$

The short term solution as pointed out in Ref. 3 gives the response of the cylinder to a plane wave (the plane wave approximation). The long term solution yields the virtual mass approximation. For short times, the plane wave approximation has been cast in the form of a matrix equation applicable to finite element analysis as follows:

$$\underline{F_s} \approx \rho c\ [A]\ \underline{U_s} \tag{11}$$

where $F_s$ is the force vector on the surface, $U_s$ is the velocity vector on the surface, and [A] is a diagonal area matrix wherein only the wetted elements are included.

For long times the virtual mass approximation has been cast as follows

$$\underline{F_s} \approx [M]\ \underline{\dot{U}_s} \tag{12}$$

where [M] is the virtual mass matrix and $\dot{U}_s$ is the acceleration of the water particle at the surface of the structure. The two solutions have been combined in Ref. 4 to obtain the doubly asymptotic approximation (DAA).

$$\underline{\dot{F}_s} + \rho c[A][M]^{-1} F_s \approx \rho c[A]\underline{\dot{U}_s} \tag{13}$$

that converges to the plane wave approximations for short times and to the virtual mass approximations for long time. A similar form may be obtained by differentiating Eq. 4. The determination of the boundaries of long and short time for the drop tests under consideration and any simplifications afforded will have to await further analysis of the data.

A useful approximation of the virtual mass of a cylindrical shell for all modes except n=o is given in Ref. 5 as

$$(m_v)_n = \rho\frac{R}{n} \tag{14}$$

where $\rho$ is the density of water, R is the radius of the shell, and n is the number of circumferential wavelengths.

Consider now the case for an infinite cylindrical shell submerged in water and excited by a plane transverse step-wave. Figure 1 represents the radial velocity at the line of initial impact (from Ref. 3) as a function of time normalized by the passage time of the step wave over the cylinder, i.e., ct/a=2 is the time when the wave has just passed over the cylinder. This

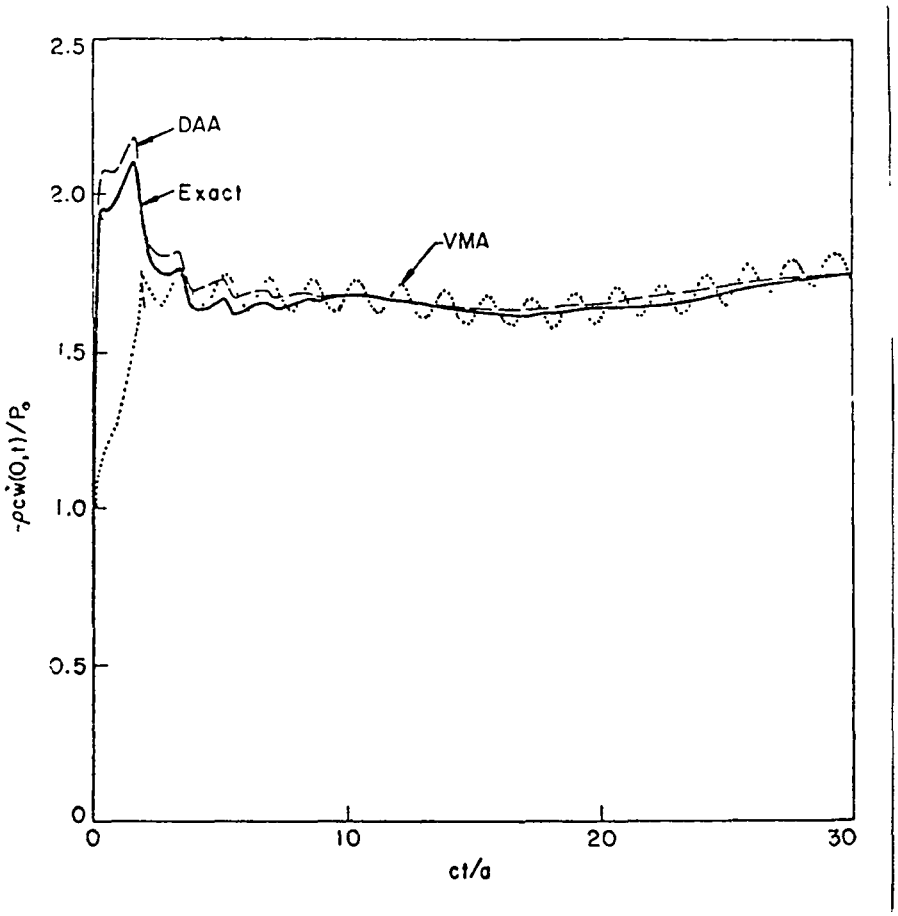


**FIGURE 1. RADIAL VELOCITY RESPONSE AT THE LINE OF INITIAL CONTACT BETWEEN AN INFINITE STEEL CYLINDRICAL SHELL SUBMERGED IN WATER AND A PLANE TRANSVERSE STEP-WAVE.**

figure presents a comparison of the DAA, the virtual mass approximation (VMA), and an exact solution. We note that in the early time the DAA gives a reasonable approximation to the peak response of the cylinder. However, the virtual mass approximation which we previously ascertained was a long time solution greatly underestimates the peak response. Although we have not yet firmly established the reason for the underestimation, it appears that we have included virtual mass for portions of the shell that have not as yet felt the step-wave and, therefore, the

virtual mass is overestimated*. In any event, it appears that there is an initial period in the response for which the virtual mass approximation alone is not valid. We also note that the virtual mass approximation tends to oscillate about the exact solution at times following the passage of the wave over the cylinder. These oscillations are again not physical and result from the fact that this approximation provides no acoustic radiation damping. The doubly asymptotic approximation (DAA) that includes a radiation damping (short time) term in addition to the virtual mass (long time) term appears to provide a reasonable estimate of the behavior for both short and long time and, in particular, provides a good estimate of the peak response. We will continue to review the literature and to exercise simple models in order to define appropriate hydroelastic corrections to the forcing functions.

Let us now return to the analysis of the pressure traces measured in the drop test of the quarter scale FWC at NSWC.

## 3. Quarter Scale Pressure Traces

Consider the pressure and displacement traces for configuration IV as presented in Fig. 28, NASA memo ED22-84-144. For times following the cavity collapse pressure pulse there are oscillations in both the pressure and displacement traces that have approximately the same period and are either in phase or 180° out of phase. If the traces are 180° out of phase, it would suggest that the pressure results from accelerations of the water applied by the vibrating case. To test this hypothesis, we attempt to determine the peak-to-peak pressure fluctuations from the displacements. The magnitude of the pressure is then

$$P = (m/A)\ a = -(m/A)\omega^2\delta \qquad (15)$$

---

*Virtual mass is determined from a potential flow solution of the flow around the body, i.e., the body is completely wetted.

where m/A is the virtual mass of water per unit area as obtained from Eq. 14, a is the local acceleration, $\omega^2$ is the frequency of vibration, and $\delta$ is the amplitude of vibration.

Prior to estimating the pressure fluctuations, we wish to determine whether this virtual mass coupled with the original mass of the cylinder gives a reasonable estimate of the period of vibration of the cylinder in the ring out period following the cavity collapse pulse. The weight of the quarter scale FWC segment is

$$\frac{96}{5 \times \pi \times 3} = 2.04 \ \#/ft^2$$

The virtual mass for 2 to 5 modes is obtained from Eq. 14 as

| Number of Circumferential Waves | Virtual Mass $\#/ft^2$ |
|---|---|
| 2 | 46.8 |
| 3 | 31.2 |
| 4 | 23.4 |
| 5 | 18.7 |

The natural frequencies in air determined from a finite element analysis of the model for each of its configurations are given in Table 1. The frequencies for each of these modes in water including the virtual mass are also presented in the table.

A set of pressure and displacement traces for configuration III is reproduced from Fig. 27 of ED22-84-144. Figure 28 contains a similar set for configuration IV and the final two figures are a corresponding pressure and a typical displacement from configuration I. An estimate of the period of vibration in the ring out portion of both configurations III and IV is .075 sec which corresponds to a frequency of 13 Hz. This frequency compares favorably with the mode 3 response of the QSFWC when

TABLE 1. NATURAL FREQUENCIES OF QSPWC WITH AND WITHOUT VIRTUAL MASS.

| | NATURAL FREQUENCIES (Hz) | | | |
|---|---|---|---|---|
| | FEA (No Virtual Mass) | | Adjusted for Virtual Mass | |
| Mode | Config. I & II | Config. III & IV | Config. I & II | Config. III & IV |
| 2 | 227 | 44 | 46 | 9 |
| 3 | 222 | 55 | 54 | 14 |
| 4 | 187 | 101 | 53 | 28 |
| 5 | 217 | 110 | 68 | 34 |

virtual mass is considered. The period of vibration in Fig. 29 is .017 sec or 59 Hz. This is very close to the predicted value for mode 3 and 4. It therefore appears that the simplified representation of the virtual mass is appropriate for the late stage ring out portion of the pressure trace.

Let us now use the displacement data coupled with this frequency in Eq. 15 to predict the pressures associated with the motion of the ringing case. In all cases, we will use peak-to-peak deflections and compare those with peak-to-peak pressures. The time segment used is indicated on the appropriate figure.

$$P_{III} = \frac{31.2}{32.2} \times \left(\frac{.4}{12}\right) \times \left(\frac{2\pi}{.075}\right)^2 \times \frac{1}{144} = 1.5 \text{ psi}$$

$$P_{IV} = \frac{31.2}{32.2} \times \left(\frac{.15}{12}\right) \times \left(\frac{2\pi}{.075}\right)^2 \times \frac{1}{144} = .6 \text{ psi}$$

$$P_{I} = \frac{31.2}{32.2} \times \left(\frac{.044}{12}\right) \times \left(\frac{2\pi}{.017}\right)^2 \times \frac{1}{144} = 3.4 \text{ psi}$$

The following table compares the pressure predicted from hydroelastic effects with that actually measured.

| | Predicted Pressure During Ringing (psi) | Measured Pressure During Ringing (psi) |
|---|---|---|
| Configuration III | 1.5 | 7 |
| Configuration IV | .6 | 9 |
| Configuration I | 3.4 | 3 |

In both configurations II and IV, the calculated hydroelastic pressure is well below the measured pressure indicating the presence of some other effect. We suspect that this is case strain. The pressure predicted for configuration I is, however, approximately correct leading us to believe that further investigation of the pressures from the stiff configurations I and II is warranted. If further investigation shows that the displacements are in fact 180° out of phase with the pressures, then these pressure traces may be the appropriate ones for the finite element analysis.

## REFERENCES

1. "Transient Flexual Vibrations of Shiplike Structures Exposed to Underwater Explosions," JASA, Vol. 48, No. 1, 1970, p. 178.

2. Mnew, Ye N. and Pertsev, A.K., "Hydroelasticity of Shells," Ship Construction Publishing Clearinghouse, Leningrad, 1970, Translation FTD-MT-24-119-71, Air Force Command Foreign Technology Division.

3. Geer. T.L. "Transient Response Analysis of Submerged Structures," in Finite Element Analysis of Nonlinear Structural Behavior, ASME AMD, Vol. 14, 1975.

4. Geer. T.L. "Residual Potential and Approximate Method for Three Dimensional Fluid Structure Interaction Problems," JASA, Vol. 49, No. 5, May 1971.

5. Klosner, J.M., "Response of Shells to Acoustic Shocks," Shock & Vibration Digest, Vol 8, No. 5, pp. 3-13.

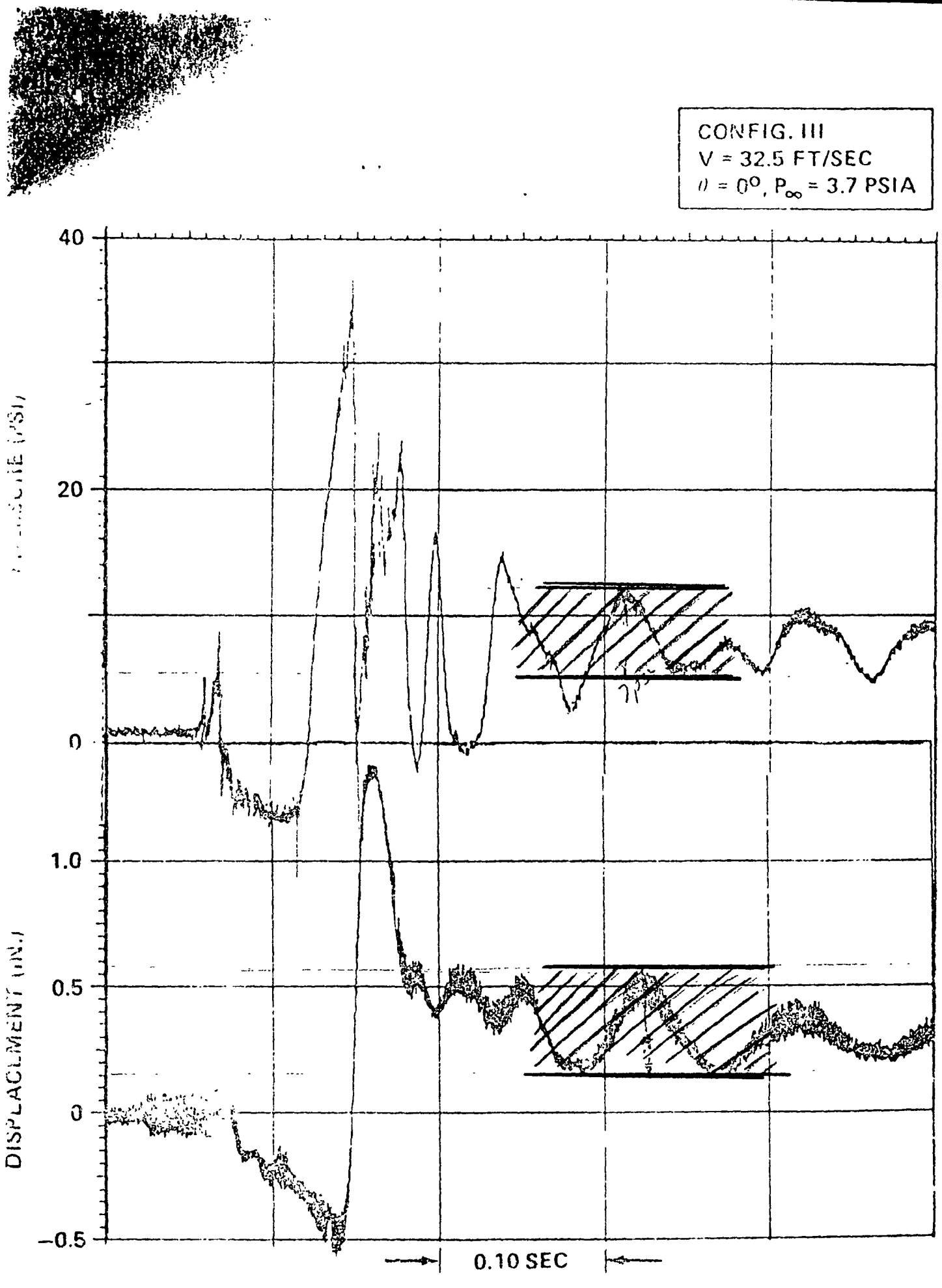


FIGURE 27. PRESSURE - DISPLACEMENT CORRELATION

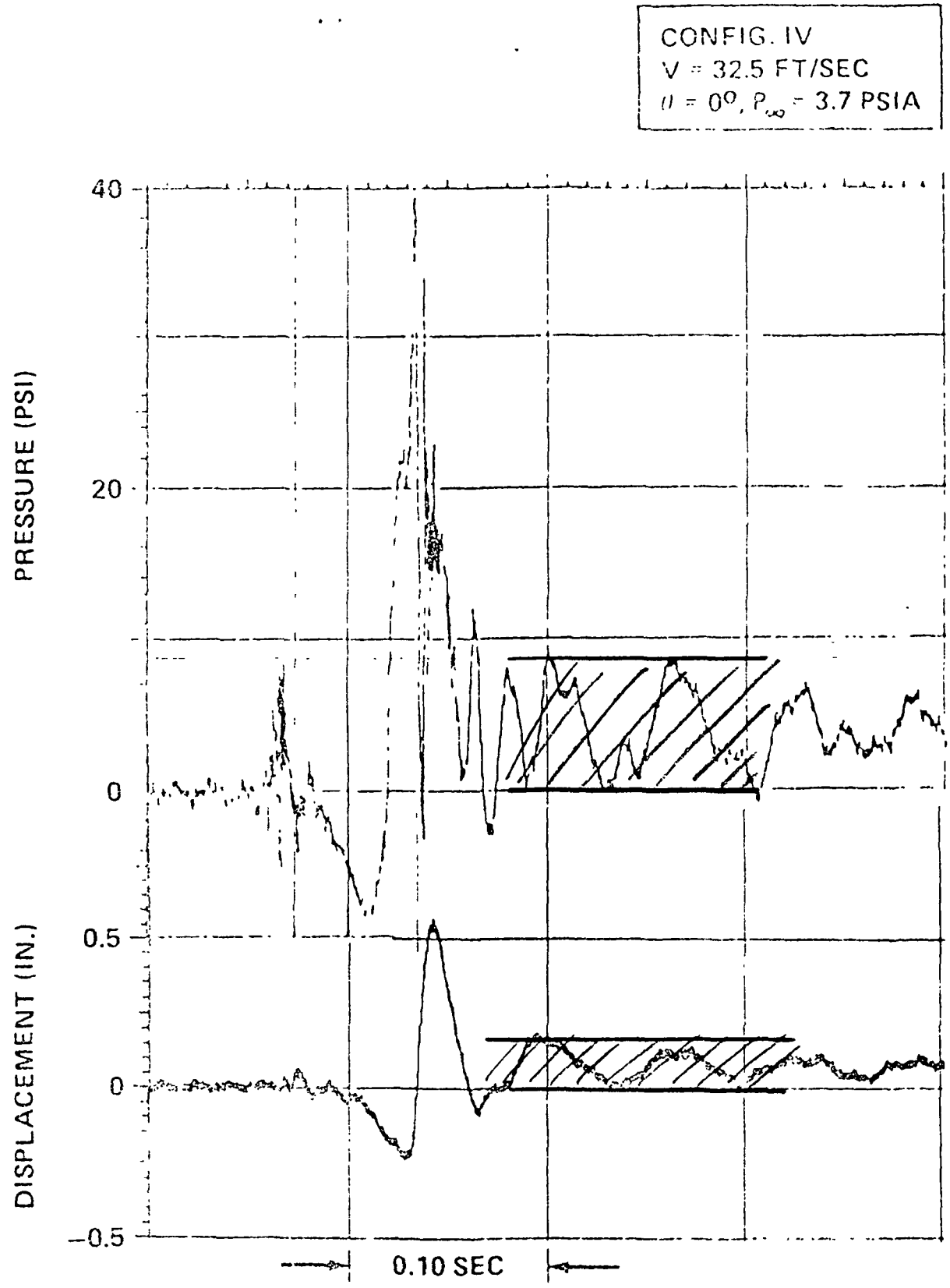


FIGURE 28. PRESSURE - DISPLACEMENT CORRELATION

ED4042

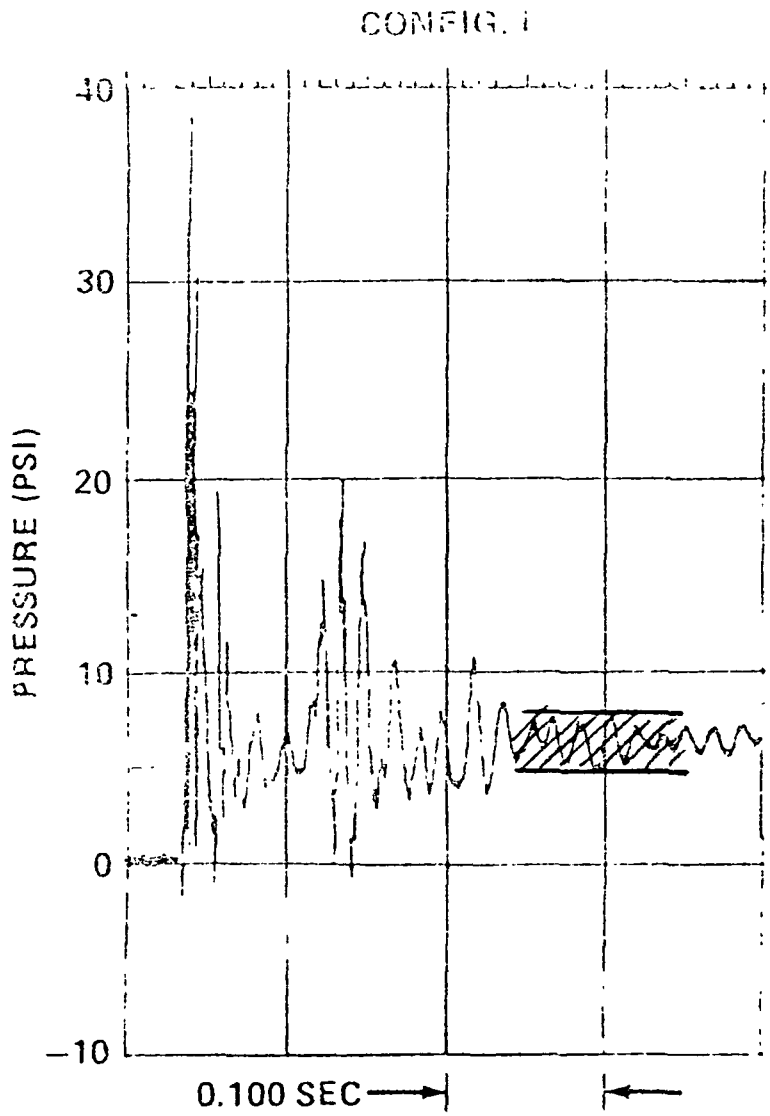


FIGURE 29. CAVITY COLLAPSE PRESSURE - EFFECT OF END CONDITIONS

TEST 84-1-02 CAVITY COLLAPSE (FILTERED)

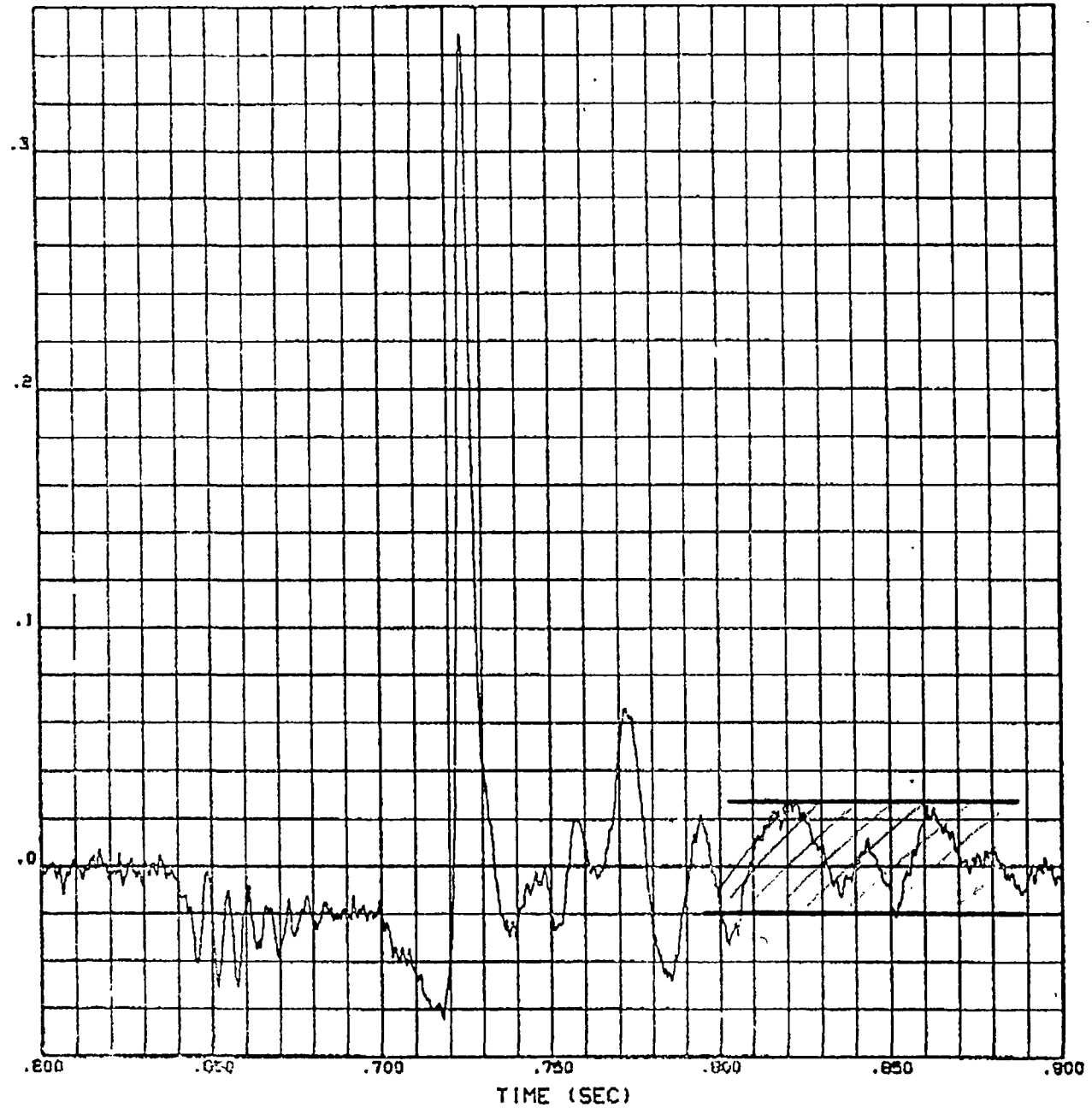


D
1
3



5 of 10

MFR05345

NASA CONTRACT NO. NAS8-35326 BBN JOB NO. 05345 05/31/84

| | TOTAL CONTRACT FUNDS | MAY MONTH TO DATE | INCEPTION TO DATE | REMAINING FUNDS |
|---|---|---|---|---|
| TOTAL LABOR | 60170 | 5063 | 45092 | 15078 |
| TOTAL OVERHEAD | 65931 | 5513 | 49767 | 16164 |
| TOTAL TRAVEL | 7974 | 0 | 13826 | -5852 |
| TOTAL DIRECT MATERIAL & HANDLING | 0 | 0 | 749 | -749 |
| TOTAL ODCS'S | 0 | -27 | 827 | -827 |
| TOTAL COST & OVERHEAD | 134075 | 10549 | 110261 | 23814 |
| G&A | 48359 | 3850 | 40312 | 8047 |
| TOTAL ESTIMATED COST | 182434 | 14399 | 150573 | 31861 |
| FEE | 16286 | 1303 | 12866 | 3420 |
| TOTAL ESTIMATED COST & FEE | 198720 | 15702 | 163439 | 35281 |